ERDC/EL SR-16-1

Environmental Laboratory

US Army Corps of Engineers®
Engineer Research and Development Center

ERDC
INNOVATIVE SOLUTIONS for a safer, better world

Environmental Consequences of Nanotechnologies

Nanomaterial Dispersion/Dissolution Characterization

Scientific Operating Procedure SOP-F-1

Lesley Miller and Mark Chappell

May 2016

Nanomaterial Dispersion/Dissolution Characterization

Scientific Operating Procedure SOP-F-1

Lesley Miller and Mark Chappell

Environmental Laboratory
U.S. Army Engineer Research and Development Center
3909 Halls Ferry Road
Vicksburg, MS 39180-6199

Final report

Prepared for U.S. Army Corps of Engineers
Washington, DC 20314-1000

Abstract

Evidence suggests that a material's dispersion and dissolution behaviors may be crucial to understanding the material's environmental risk. Since exposure risks are directly determined by the environmental fate of nano silver (nAg), extensive efforts have been put forth in elucidating the behavior of these materials in natural systems. Thus, it is important to understand the different metrics that can be used to represent nanoparticles (NPs) in a system.

Given the connection between a material's dispersion and dissolution kinetics, a protocol is presented to measure the dissolution kinetics of nanomaterials using a simple 48-hour experimental protocol that utilizes environmentally representative waters as well as non-destructive analytical techniques. Protocols for the simultaneous measurement of the nanoparticle dispersion properties are also presented. When used with the appropriate equations listed in this scientific operating procedure, data derived from these simple experiments can provide fundamental information about the behavior of nanoparticles in different environments.

Contents

Figures and Tables

Figures

Tables

Preface

This special report describes a Scientific Operating Procedure (SOP) and outlines the recommended steps to perform dispersion and dissolution testing to nanomaterials in a laboratory environment. The research was performed by Lesley Miller and Mark Chappell, U.S. Army Engineer Research and Development Center (ERDC) – Environmental Laboratory (EL), Vicksburg, Mississippi. Funding was provided by the Environmental Quality and Installations Program.

This study is part of the Environmental Quality/Installations (EQ/I) Research and Development Program focus area directed by Dr. Jeff Steevens. This focus area is under the direct supervision of Alan Kennedy, ERDC-EL, and under the general supervision of Dr. Elizabeth Ferguson, Technical Director for Military Munitions in the Environment, ERDC-EL. At the time this report was prepared, Dr. Jack Davis was Deputy Director, ERDC-EL and Dr. Beth Fleming was Director, ERDC-EL. COL Bryan S. Green was Commander of ERDC and Dr. Jeffery P. Holland was Director of ERDC.

1 Introduction

The Standard Operating Procedure (SOP) described herein for assessing the properties of nanotechnologies was developed under Task 2: Optimized Scientific Methods of the ERDC/EL Environmental Consequences of Nanotechnologies research program. The primary goal of this Task was to develop robust SOPs for investigating the environmental health and safety (EHS) related properties of nanotechnologies including nanomaterials and products incorporating nanomaterials.

This SOP describes a technique and guidance for assessing the dispersion and dissolution behaviors and properties of a nanomaterial.

2 Background

2.1 Thermodynamic considerations for dissolution

2.1.1 Ionic species formation and thermodynamic expressions

Dissolution refers to the transfer of solid-phase components to liquid phase, usually in simplistic ionic forms or species. Thermodynamically, species types formed and resulting inter-species transformations are represented as Scheme 1, where M represents the metal in elemental or oxidized forms; n+ represents the positive charge of the metal; x and y represent the stoichiometric coefficients of M and O as well as other anionic ligands (as influenced by the metal charge or n+). This scheme shows that overall, NP dissolution can drive the formation of a variety of ionic species containing their own reaction constants (K_i) that must be satisfied as well. The different equilibrium reactions are shown for (1) oxidation of metallic species, driven by a redox potential (Eh), where Eh represents the oxidation reaction of the metallic NP that is coupled with the reduction of molecular oxygen to water; (2) dissolution of metal oxides, as dictated by a solubility constant (K_{sp}), which kinetically is equivalent to the time-dependent system at steady-state; (3) Hydrolysis of dissolved metal ions, as driven by a hydrolysis constant (K_{H2O}); (4) pH dependent species formations, driven by acid and base dissociation constant (K_a, K_b, where equation is shown converting K_b to K_a); and (5) precipitation of secondary species (K_{sp2}). The distribution of ionic species and their associated reaction constants thermodynamically drive dissolution processes. In particular, the hypothetical species shown here are related to metals and metal oxides, but a similar theory may work for derivatized carbon materials such as with carboxyl, hydroxyl, or amino groups.

Scheme 1: Potential chemical reactions and ionic species formation associated with solid-phase dissolution

Redox reaction

$$M^0_{(s)} \xrightleftharpoons{O_2} M^{n+}_x O_{y/n(s)} \qquad E_h = -RT/nF \ln K_{eq}$$

Dissolution

$$M^{n+}_x O_{y/n(s)} + \alpha H^+ \rightleftharpoons M^{n+}_x + \beta H_2O \qquad K_{sp} = \frac{(M^{n+})^x}{(H^+)^\alpha}$$

Hydrolysis

$$xM^{n+} + \beta H_2O \rightleftharpoons M^{n+}_x (OH)^0_{y/n} + \alpha H^+ \qquad K_{H_2O} = \frac{(M^{n+}_x (OH)^0_{y/n})(H^+)^\alpha}{(M^{n+})^x}$$

pH-dependent species formation

$$M^{n+}_x (OH)^0_{y/n} + \beta H_2O \rightleftharpoons M^{n+}_x (OH)^-_{(y+1)/n} + \alpha H^+ \qquad K_{a_1} = \frac{(M^{n+}_x (OH)^-_{(y+1)/n})(H^+)^\alpha}{M^{n+}_x (OH)^0_{y/n}}$$

$$M^{n+}_x (OH)^0_{y/n} + \alpha H^+ \rightleftharpoons M^{n+}_x (OH)^+_{(y-1)/n} + \beta H_2O \qquad K_{b_2} = K_w / K_{a_2}$$

Precipitation

$$M^{n+}_x (OH)^0_{y/n(aq)} \rightleftharpoons M^{n+}_x O_{y/n(s)} \qquad K_{sp_2} = (M^{n+}_x (OH)^0_{y/n}$$

2.1.2 Solubility laws

As shown above, the solubility of the NP species is predicted by the Ksp. In turn, thermodynamics predicts that the Ksp is influenced by three important solubility laws: salt, common-ion, and complexation effects.

The **Salt effect** represents the influence of ionic strength on the activity of the ionic constituents controlling the total solubility or Ksp of the NP. Here, activity (α in mol L^{-1}) is

$$a = gC_i \tag{1}$$

where, γi = activity coefficient for species i and m_i = concentration of species i in mol L^{-1}. Typically, α is assumed = C_i but in the presence of salt, the two values are different due to the effect of the solution ionic strength (I), which is defined as

$$I = 1/2\sum_{i=1}^{n} C_i z_i^2 \tag{2}$$

where C_i = concentration (mol/L) of ith ion, z = ionic charge. The Debye-Huckel equation predicts the impact of I on γ as

$$\log \gamma = \frac{-0.509 z_i^2 \sqrt{I}}{1 + 0.9843\sqrt{I}} \tag{3}$$

Thus, the solubility reaction in Scheme 1 is rewritten as:

$$K_{sp} = (C_{M^{n+}} \gamma_{M^{n+}})^x (C_{OH} \gamma_{OH})^y \tag{4}$$

Equations 1,2, and 3 predict that an increase in I decreases γ, which in turn results in an increase in Ksp. Furthermore, salts of different ionic compositions (e.g., monovalent vs. divalent) will further suppress γ and further enhance Ksp. This consideration must be taken into account when investigating the influence of salt background on NP solubility.

The **Common-ion** effect refers to the decreased solubility of an NP due to the addition of a “common” ion, or in other words, the same ion released due to dissolution. For example, if nAg is dissolved in a solution containing background AgCl, then the common-ion effect can be represented in the equilibrium expression as:

$$\frac{K_{sp}}{(OH^-)^y} = (M^{n+})^x \tag{5}$$

Equation 6 shows that by increasing the concentration of M^{n+} in solution impedes the release of OH^- ions in order to satisfy the equilibrium conditions, so in essence the Ksp decreases.

The **Complexation** effect refers to increase in solubility due to the “complexation” of the dissolved species with a different ionic species, such as organic chelators, or other ion pairs. These form soluble ion pairs in solution, which as a result, decrease (M^{n+}) in solution because it was used to form a different species. As a result, the mineral is energetically driven to release more ions by dissolution (i.e., increase Ksp) to reestablish equilibrium ratios of ions. By forming ion pairs, the concentration of ionic solute decreases, thus promoting increased dissolution. This effect is particularly important for systems containing chloride ions, which can enhance the solubility of minerals due to ion pairing.

2.2 Dissolution kinetics and equilibrium

Dissolution can be defined in terms of equilibrium as

$$K_{sp} = K_{eq} = \frac{(M^{n+})^x (OH)^{y/n}}{(M_x(OH)_{y/n})} = \frac{k_f}{k_b} \quad (6)$$

where k_f and k_b represent the forward and backward rate constants for a dissolving NP, with the forward reaction described by dissolution and the backward reaction described by precipitation. At steady state, the ratio between k_f and k_b is constant. In the equilibrium expression, at the solid ($M_x(OH)_{y/n}$), which here refers to the particle concentration, is traditionally set equal to one. Yet, if an NP suspension is below saturation (<Ksp), then this assumption may not be valid, and dissolution kinetics (leading to steady state) is dependent on NP suspension concentration.

Table 1 shows the different conventions that can be adopted for describing NP concentrations. Mass concentration represents concentration as the same units as dissolved ions but gives no information regarding the dimensionality of the particles in suspension. Number density (Ns) is useful for describing the number of particles in a volume of solution, based on the size of the particle (current equation assumes spherical particle shape), which normalized by Avogadro's number, gives a calculation of suspension molarity. Current evidence suggests that toxic responses from dissolved ions released by soluble NPs demonstrate dose-response curves with respect to higher NP surface area of the smaller particles (Kennedy et al., 2014), while toxicity associated with non-dissolving NPs may demonstrate opposite trends with respect to Ns. In any case, this discussion demonstrates that the different ways to represent NP suspensions must be carefully considered in dissolution experiments.

Table 1. Different metrics and formulas for representing concentrations in NP dispersions.

Unit	Equation
Mass concentration	C/MM
Number density (Ns)	$C\,\rho_b N_A / 6\pi d^3$
Specific surface area (SSA)	$6C/\rho_b d$

C = bulk concentration (mg L^{-1}), MM = molar mass, ρ_b = bulk density (g cm^{-3}), N_A = Avogadro's number, d = particle diameter (nm)

Because a nanoparticle dispersion represents a mixture of two physical phases, there are energetic tendencies toward separating the solid phase material from the liquid (typically, aqueous phase in environmental conditions) and flocculate. In an aqueous system, kinetics of diffusion-limited flocculation for particles is classically represented as a second-order reaction:

$$\frac{dN}{dt} = k_2 N_0^2 \tag{7}$$

where N_0 = the initial particle number density (m^{-3}), and k_2 = initial 2nd order particle collision constant. For particles bearing repulsive electrostatic charge, potential-limited flocculation kinetics can be represented as (Ottewill 1990)

$$\frac{dN}{dt} = \frac{k_2 N_0^2}{W} \tag{8}$$

where W = Fuch's stability ratio. Thus, Smoluchowski's condition of non-interacting particles (equation 8) is met when W = 1. Note that at initial time periods, when N_0 = N, N is inversely related to particle volume (r^3) as (Kimijima and Sugimoto 2004)

$$N = \frac{V_m C_p}{r^3} \tag{9}$$

where V_m = particle molar volume, C_p = total mass concentration. Also, assuming a spherical particle, the particle volume = $4/3\pi\, r^3$. Equations 9 and 10 show the inverse relationship between N and particle volume. At a constant mass concentration, equation 10 predicts that an increase in the particle volume results in a decreased N, presumably due to flocculation processes. Thus, k_2 is described as a second-order rate constant – the classical mode attributed to flocculation by coagulation. The parameter W is related to the electrostatic interaction between particles, representing the relative magnitude of repulsive forces that arise from overlapping but similarly charged double layer volumes. This distance can be described in terms of the value of the Debeye length (κ) as proportional to $I^{1/2}$, where I = system ionic strength. Thus, at constant pH, a useful approximation of the nAg dispersion stability is (Morrison and Ross 2002)

$$\log W = -0.5 \log I + k_2 \tag{10}$$

Equation 11 predicts that dispersions exposed to increasing electrolyte concentration will begin to destabilize, due to increasing κ (in units of m^{-3}), and promote flocculation.

Particle dissolution, on the other hand, is treated theoretically as a completely separate phenomenon with respect to particle dispersion behavior. The general equation describing the relationship between particle size (*r*) and dissolution is (Langberg and Nilmani 1996)

$$\frac{dm}{dt} = k_m \Delta C \tag{11}$$

where m = particle mass, ΔC represents the difference between the solid's maximum solubility (defined at equilibrium by the solid's solubility constant, K_{sp}) and the concentration in solution with time (C(*t*)) or = K_{sp} - C(*t*). The parameter k_m represents the particle dissolution rate constant, which accounts for the relative solute diffusion constant, system mixing energy, and system viscosity (Langberg and Nilmani 1996). According to equation 12, a decrease in particle mass (and corresponding loss of particle size) from dissolution is dependent on the magnitude of difference between the solute concentration and its maximum solubility in aqueous solution (K_{sp}). Thus, change in particle mass (and corresponding size) is predicted to remain constant when solute concentration reaches saturation, or maximum solubility (assuming no secondary phases or precipitates form), and according to equation 1, particle flocculation will also cease.

Equation 12 can be expanded as the Noyes-Whitney equation to include particle properties as:

$$\frac{dm}{dt} = k_m A\left(K_{sp} - C(t)\right) \tag{12}$$

where, m = mass of dissolved material, A = the particle surface area (calculated as 3/r) in contact with the surrounding medium (Hageman, 2006). This equation indicates a direct relationship between the change in particle mass loss (from dissolution) and the particle surface area. Thus, if the term (K_{sp} – C(t)) remains constant, then the change in particle mass is directly related to the particle surface area. Equation 13 predicts that smaller particles will exhibit a larger dissolution than larger particles.

It is important to standardize the procedures by which a nanomaterial's behavior in dissolution and dispersion systems is assessed. In an effort to standardize the process for doing so, ERDC has developed the present protocol to guide users in creating and analyzing such systems in environmentally representative laboratory conditions.

3 Scope

This SOP is used to measure the dissolution kinetics of nanoparticle dispersions for a 48 hour time period. Because nanoparticle dissolution kinetics are generally dependent on the properties of the nanoparticle dispersions, this protocol is designed to measure dispersion properties simultaneously to particle dissolution. The protocol presented here was developed based on our experience with aqueous nanosilver dispersions (Chappell et al, 2011), yet time period and dissolution measurements can be modified as needed.

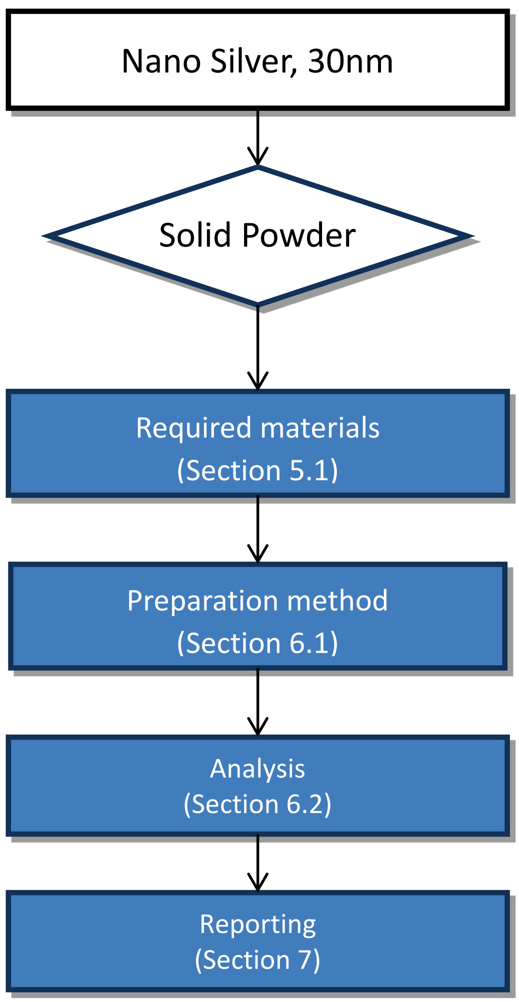

4 Terminology

4.1 Related Documents

- E1617 Practice for Reporting Particle Size Characterization Data
- ERDC SOP-T-1
- ENV/JM/MONO(2001)9 OECD SERIES ON TESTING AND ASSESSMENT NUMBER 29
- ENV/JM/MONO(2008)25 SERIES ON TESTING AND ASSESSMENT NUMBER 98

4.2 Definitions

- agglomerate, n—in nanotechnology, an assembly of particles held together by relatively weak forces (for example, Van der Waals or capillary), that may break apart into smaller particles upon processing, for example.

4.3 Acronyms

- DLS – Dynamic Light Scattering
- ICP-MS – Inductively Coupled Plasma-Mass Spectrometry
- TOC – Total Organic Carbon
- EC – Electrical conductivity
- ISE – Ion specific electrode
- DI – De-ionized

5 Materials and Apparatus

5.1 Materials

- Max Q 7000 orbital shaker (Thermo Scientific, model 3540-5) Erlenmeyer flasks (250 mL) with rubber stoppers
- Aluminum foil
- Double de-ionized water
- Moderately Hard Reconstituted Water (MHRW)
- Instant Ocean©
- pH calibration standards (pH 4,7,10)
- Electrical Conductivity (EC) calibration standards (range is dependent on EC tests of background salts)
- Silver Ion Specific Electrode (ISE) calibration standards
- Low Density Polyethylene (LDPE) test tubes (volume capacity >15 mL)
- 96-well, clear, flat-bottom, polystyrene microplates (Fisherbrand)
- 12mm polystyrene cuvettes (Malvern Instruments, DTS 0012)
- Polycarbonate 6 mL ultracentrifuge tubes (ThermoFisher, 50867083)

5.2 Apparatus

- Fisher Scientific Accumet combination pH probe
- Fisher Scientific Accumet pH/EC/ISE meter
- Fisher Scientific Accumet electrical conductivity (EC) probe (1 cm^{-1})
- Volumetric pipettes
- Orion ISE probe (with internal reference)
- Max Q 7000 orbital shaker (Thermo Scientific, model 3540-5)Thermo Sorvall MTX-150Ultracentrifuge
- Fisher Multiskan microplate reader
- Perkin Elmer Elan DRC-II ICP-MS equipped with a MiraMist nebulizer

6 Procedure

- Disperse nanomaterials (SOP-T-1) in desired background matrix (de-ionized water, simulated fresh water, simulated marine water) in triplicate in 250 mL flasks previously covered in aluminum foil to prevent incidental dissolution due to photooxidation. Once dispersions are made, plug flasks with rubber stoppers to prevent water loss through evaporation.
- Immediately place flasks in orbital shaker, and shake at approximately 60 revolutions per minute (rpm) for a total of 48 hours.
- Sample the suspension with time, choosing at least five sampling points (sufficient for kinetic modeling) over a 48 hour period. Typical sampling is done at hours 1, 6, 24, 29, and 48.
- Immediately before sampling, measure pH and EC (calibrate probes based on manufacturer instructions) of each flask. Sample each flask by removing 5 mL into labeled vials.
- Analyze each sample as described below.

6.1 Sample Preparation

Preparations are made for measurement of both nanoparticle dispersion properties as well as constituent solute released by dissolution. Dispersion properties are measured by turbidity and DLS measurements to determine the total particle concentration and aggregate distribution, respectively. Dissolution is determined by both total and ionic silver (Ag^+) measurements conducted by ISE or ICP-MS both before and after ultracentifugation. Information obtained from these two dissolution measurements can be used in geochemical speciation modeling to estimate the distribution of dissolved species.

- Subsamples will be divided as follows:
    - ISE measurement before further processing
    - 250 µL pipetted into 96-well microplate for turbidity measurement
    - 1 mL into four-sided cuvette for DLS measurement
    - 1 mL (diluted with 9 mL of 1% Nitric Acid) into glass vial for ICP-MS measurement (total metal concentration)
    - 1.5 mL for ultracentrifugation

6.2 Analysis

6.2.1 Dissolved Ag by ISE measurement

1. Calibrate ISE probe following manufacturer instructions. Example calibration curve is given in Figure S.2.
2. ISE measurement in sample: Place ISE probe in the subsample and allow the measured voltage to stabilize before recording measurement. However, do not add ionic strength buffer as recommended by the manufacturer because the added salt will directly impact the state of the nanoparticle dispersion and thus interfere with ISE measurement. Instead, the dissolved Ag^+ activity concentration can be calculated by multiplying the activity of Ag^+ (α_{Ag}, as obtained by the ISE measurement) by the corrected single ion activity coefficient ratio (γ_C/γ_S), where γ_S =Ag^+ activity coefficient calculated from the standards (at I = 0.1 M, γ_S = 0.80), and γ_C = Ag^+ activity coefficient based on the ionic strength contributed by background salt and equilibrium polyelectrolyte in the dispersion (Chappell et al., 2011). Because of the high salt content in the ionic strength buffer, the single-ion activity coefficients were calculated using the Davies equation:

$$\log \gamma = -0.5z^2\left(\frac{I^{1/2}}{1+I^{1/2}} - 0.3I\right) \tag{13}$$

where the terms are defined the same as in equation 3.

6.2.2 Turbidity measurement (dispersion)

Pipet subsample aliquots and background blank aliquots into the 96-well microplate.Cover with microplate plastic lid. Analyze the microplate at 620 nm.

6.2.3 DLS measurement (dispersion)

One milliliter of the sample is placed in a polystyrene cuvette and measured using the Malver Zetasizer Nano ZS. The Zetasizer is designed for automated optimization of parameters for measurements. The instrument utilizes a 173° backscatter angle, and determines automatically the measurement position of the lens. The number of scans is also determined automatically by statistically analyzing each sample. A general purpose analysis method is applied to the data by the Zetasizer software, and the user evaluates quality reports provided by this analysis to determine best fit models.

6.2.4 Total and ionic Ag dissolution measurement.

1. Perform ICP and ISE measurements on the suspension as described Section 6.1 and Section 6.2.1.
2. Ultracentrifuge suspension at 100,000 x g for 30 minutes. Pipette the top 1 mL of supernatant into a vial diluted with 9 mL of 1% Nitric acid for ICP-MS measurement of metals (USEPA Method 6020).

7 Reporting

7.1 Analysis of Results

7.1.1 Calculating total particle concentration from turbidity measurements

Particle concentration is calculated from a previously constructed calibration curve (concentration vs. absorbance at 620 nm).

7.1.2 Calculating the intensity-averaged particle diameter from DLS measurements

The intensity-averaged particle diameter (nm) is calculated from the sum of the integrated scattered intensity at each size increment. Before integrating the DLS size distribution data, the intensity is normalized by the highest intensity value. Thus, the intensity-weighted particle diameter (Σd) is calculated by:

$$\sum d = d_1 I_1 + d_2 I_2 + \ldots d_i I_i \tag{14}$$

where d_i = diameter size increment and I_i = percent intensity of the size increment.

7.1.3 Calculating surface area and number density of nanoparticle dispersion

See Table 1.

7.1.4 Kinetic modeling of dispersion-dissolution data

7.1.4.1 Aggregation modeling

The simplest approach to modeling aggregation data is to use the integrated second-order model:

$$\frac{1}{N} = \frac{1}{N_0} + k_2 t \tag{15}$$

where N = particle number density (m^{-3}) with time (t), N_o = initial particle number density at t = 0, and k_2 = initial second-order particle collision constant (t^{-1}) as defined in equation 8. A line fitted through the a plot of $1/N$ vs. t will give a slope = k_2 and a y-intercept = $1/N_o$.

Table 2. Intensity-averaged particle diameter, Σd (equation 14), calculated from the size distribution of nAg suspensions in different media, as determined from the autocorrelation function obtained from DLS measurements

Media	Time (h)	Intensity-weighted particle diameter (nm)
Reference	0	40±1
DI	0	42±2
	24	38±2
MHRW	0	245±91
	1	182±31†
	24	215±46†
CS	0	377±138
	1	332±43†

† high error of estimate due to poor data quality

7.1.4.2 Dissolution modeling

The simplest approach is to model dissolution data using a first-order kinetic rate law:

$$\ln[M^{n+}] = k_1 t + \ln[M_0^{n+}] \tag{16}$$

where $[M^{n+}]$ = dissolved metal concentration and k_1 = first-order dissolution rate constant (t^{-1}). A plot of $\ln[M^{n+}]$ vs. t will give a slope = k_1 and a y-intercept = $\ln[M^{n+}{}_o]$.

7.1.4.3 Dissolution modeling using the Noyes-Whitney equation (equation 13)

The integrated form of equation 13 is:

$$m(t) = k_m A t\left(K_{sp} - C(t)\right) + c_1 \tag{17}$$

where m = particle mass, c_1 = y-intercept of the line, A = particle-solution surface interfacial area, K_{sp} = particle solubility constant, $C(t)$ = dissolved metal concentration (with time), and k_m = Noyes-Whitney particle dissolution rate constant. A plot of *m* vs. *t* gives a linear plot with a slope = $k_{m.}\left(K_{sp} - C(t)\right)$ and the rate constant calculated by

$$k_{m.} = \frac{\textbf{slope} \times A}{\left(K_{sp} - C(t)\right)} \tag{18}$$

7.2 Key Results Provided

7.2.1 Particle size measurements by DLS

Corellograms for the DLS analysis (Figure 1) show that ionic background compositions from the MHRW and Crystal salt (CS) medias promoted particle flocculation (we assume) via classic suppression of double-layer repulsive forces around the charged particle surface. This is evident in the corellogram by the increased time lag (in μs) in signal fluctuations with salt concentration, which is interpreted to represent the slower diffusion coefficient associated with the "free" tumbling of larger-diameter particles. Furthermore, the presence of salts results in the transition from smooth or simple correlation functions to multi-modal functions, indicative of the development of a polydisperse colloidal system.

In terms of kinetics, it seems clear that the influence of the salts on the corellogram describing the dispersion state are nearly instantaneous; thus, preventing application of aggregation kinetic modeling to this data. The corellograms for nAg in deionized water (t = 0-24 h) are very similar to the reference material. nAg particles in MHRW (t = 0-1 h) show evidence of the formation of larger aggregates at 10^3-10^5 μs lag times, with an even proportion of the corellogram occupied by large-sized aggregates of t = 24 h. For the CS (t = 0-1 h), the corellograms show evidence for even larger aggregates, with lag times ranging from 10^3 to 10^6 μs, but the data for CS (t > 1 h) were unreliable. Figure S.1 emphasizes this point by showing the calculated uncertainty in the corellograms. Clearly, the uncertainty in the information obtained from the DLS needs to be closely monitored as media that promoted colloid aggregation and introduced error in the measurements.

Figure 1. Corellograms (obtained by DLS measurements) for nAg particles in different media at different time points.

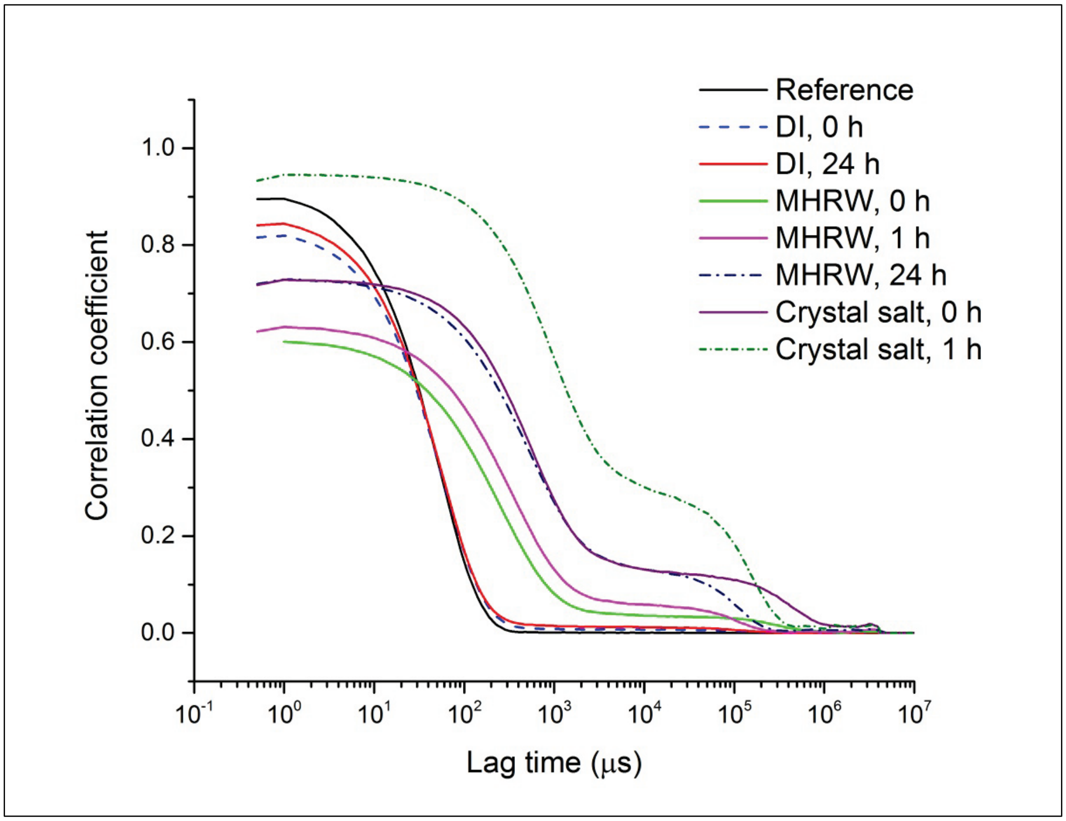

Figure 2 shows the particle characterization data interpreted from the autocorrelation function. As indicated from Figure 1, the size distribution of nAg particles in DI water was similar to that of the reference system, yet we note that there was a substantial increase in measurement error associated with this system. Stabilizing components of NPs and test media may affect the error observed in a system. Within the present sytem, particle distributions were one to two orders of magnitude larger than stated by the manufacturer.In this case, users may only be able to capture data generated at t=0h within the confines of the DLS.

The software within the Malvern Zetasizer system (research-level option) used in this study offers different options for calculating the size distributions of particles from the autocorrelation function. Here, results from two methods are presented: (i) size distribution and (ii) cumulant analysis, depending on the polydispersity of the suspension. The former was used to calculate the intensity-weighted particle diameter (Σd) of the nAg suspensions in the different matrices (Table 1). The nAg reference material was exactly 40 nm in diameter. In deionized water, Σd ranged

Figure 2. Plots showing the distribution of back-scattered signal intensity based on the calculated hydrodynamic diameter of particles in different media.

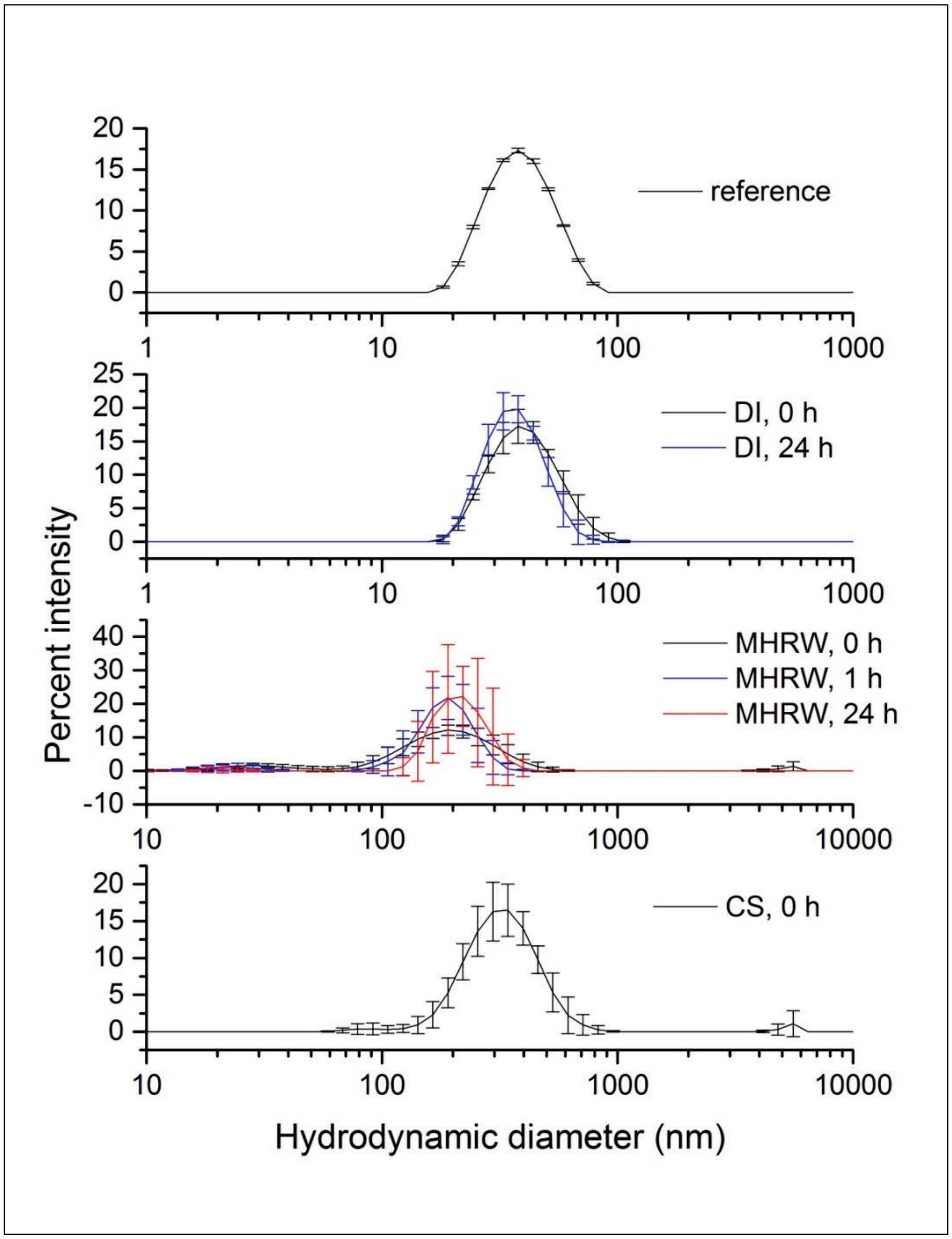

from 38 to 42 nm for t = 0-24 h, but the change was statistically indistinguishable. In MHRW, Σd ranged from 182 to 240 nm for t = 0 to 24h, indicating that the salt concentration or type promoted aggregation of nAg particles. Calculated Σd for the Crystal Salt systems ranged from 332 to 377 nm for t = 0 to 1 h. Σd estimates for nAg particles beyond t = 0 h in the MHRW and CS systems were high in error due to poor data quality.

Calculated size distributions via cumulant analysis are included in Table 2. This method is applicable for good-quality data exhibiting monodisperse side distributions. The calculated Z-average of the reference material as 36 nm, with a polydispersity index (PDI) of 0.11, indicative of a monodisperse material. While the nAg's calculated Z-average in DI water (ranging from 35 to 37 nm) was statistically indistinguishable from the reference suspension, the PDI was significantly higher, suggesting the beginnings of destabilizing the suspension due to dilution of matrix components. In CS, cumulant analysis indicated evidence aggregation resulting in the development of a polydisperse suspension. While the nAg suspensions were too polydisperse in MHRW, the suspension exhibited sufficient monodispersity in CS at t = 0 h to be analyzed by the cumulant model. The reason for this behavior is probably attributable to the high Na content of CS, which dominated the response of the particles.

Table 3. Z-averages and PDIs for nAg particles in different media based on cumulant analysis of the autocorrelation function obtained from DLS measurements

Media	Time (h)	Z-average (nm)	PDI
Reference	0	35.6±0.1	0.111±0.009
DI	0	35.3±11.7	0.188±0.038
	24	36.9±13.9	0.183±0.041
CS	0	392.8±133.4	0.423±0.034

The differences in the response of the nAg suspension can be understood theoretically by the effect of the background electrolyte on the electrostatic repulsion among particles. The simple model in equation 11 predicted the log W as a function of salt concentration given that $\kappa \alpha I^{1/2}$, and

$$I = 1/2 \sum m_i z_i^2 \tag{19}$$

where m_i = ion concentration and z = ionic valence. At the x-intercept (log W = 0), the dispersion is unstable. This point represents the counterion electrolyte concentration that flocculates the dispersion, called the critical coagulation concentration (CCC).

$$CCC = \frac{0.46 * 8.74 \times 10^{-39} \gamma^4}{z^6 A_{121}^2} \tag{20}$$

where,

A_{121}^{2} = the Hamaker interaction constant,
z = counterion valence,
γ = defined as $\gamma = \tanh \frac{ze\psi_0}{4kT}$, and
ψ =defined surface electrical potential.

Yet, these relationships are otherwise not impacted by the presence of particles (Goodwin, 2009). The CCC is represented in units of mol L^{-1} of salt and is dependent on valence of the electrolyte counter-ions. The mixed ionic composition of the MHRW, containing monovalent and divalent salts, is expected to exhibit a combined aggregation response, while the dominant monovalent composition of the CS is expected to exhibit a more homogeneous aggregated response. Thus, it is important to consider the presence and ionic composition of background electrolyte in an electrostabilized suspension.

The above emphasizes the importance of closely monitoring the quality of the particle size data, as well as the theoretical modeling used to interpret the autocorrelation function, particularly given the expected behavior of particles under different background electrolyte solutions. In our experience, different particle-size domains can be best distinguished for aggregates differing in roughly one order of magnitude. Yet, these differences are reliably distinguished if the uncertainty in the correlogram is minimal. Further manipulating the dust cutoff in the software may digitally reduce noise in the DLS data caused by larger particle sizes, but this approach is generally less reliable than additional steps to physically remove large particles, such as allowing the suspension to settle for 24 h (Chappell et al., 2009).

7.2.2 Suspension turbidity measurements

For this work, investigation was conducted on how the kinetics of nAg dispersions were modified by the presence of electrolyte and surfactant. This was done by recording both the change in particle size (d) and turbidity or attenuation of light through the suspension. This attenuation, representing the exponential decrease of the intensity of light passing through the medium, is described as

$$I_{trans} = I_0 e^{-\tau x} \tag{21}$$

where ι = turbidity of the medium (cm-1), which is directly related to the number density (N) as their individual extinction cross sections (σ_{ext}) as (Sorensen et al., 1997)

$$\tau = N\sigma_{ext} \tag{22}$$

where the extinction coefficient $\sigma_{ext} = \sigma_{abs} + \sigma_{scat}$. Assuming $\sigma_{scat} >> \sigma_{abs}$, then τ represents the number density of particles due to light scattering. If we model σ_{ext} based on Mie scattering, then

$$\sigma_{ext} = 0.25 Q_{ext} \pi d^2 \tag{23}$$

Q_{ext} is the Mie extinction coefficient and is defined as

$$Q_{ext} = 2\left[1 - \frac{2}{\rho}\left(\sin\rho - \frac{1}{\rho}(1-\cos\rho)\right)\right] \tag{24}$$

where $\rho = \dfrac{2\pi d(m-1)}{\lambda}$, λ = wavelength of scattered light, and m = ratio of refractive indices for the nanomaterial and dispersing medium. Thus, combining equations 22 and 23 and rearranging gives:

$$N = \frac{\tau}{0.25 Q_{ext} \pi d^2} \tag{25}$$

Equation 25 demonstrates the inverse relationship between particle number density and size. It explains that when the total mass of the nanomaterial is conserved, then change in *d* can only be interpreted as a change in *N*. The effects of changes in size are particularly important at the nanoscale. For nanoscale solids, an increase from one to 10 nm particle size represents a three orders of magnitude decrease in N, from 10^{12} to 10^9 particles per µL volume.

The turbidity response of the nAg suspension should provide complementary information with regard to the size of the particles. The above shows that assuming a constant mass concentration of particles, a suspension containing smaller sized particles, should exhibit a higher τ value, directly reflecting the higher *N*. This information should be taken in balance with the fact that I_{trans} is proportional to r^6, as predicted by Raleigh theory.

However, the data showed no measurable difference in τ values for the different systems tested, most likely due to the detection limits of the transmission-based technique as opposed to overlapping absorbances arising from the suspension matrix. This was confirmed by preliminary UV-vis scans so that no particular absorbance was observed for nAg particles in the range of 600 nm. It is expected that a more robust technique called the IR ratio, which represents the ratio of both transmission and light-scattering measurements (non-integrating like DLS), would be more sensitive to lower concentrations of nAg.

7.2.3 Simultaneous nAg dissolution measurements

Figure 3 shows the kinetic data collected using the ISE. Here, all three replicates are plotted simultaneously. Unfortunately, the ISE response was below the possible calibration range (<1 mg L^{-1}) of Ag concentration (Figure S2), so the concentration of Ag ions released by the particles cannot be calculated. If the ISE response is below the calibration range, users should refer to the previously recorded voltage to assess trends in ion release. However, this trend in Ag^+ release by the electrode's response can be inferred. The data shows that the recorded voltage generally ranged between 200-250 mV with time for the nAg particles suspended in DI water and MHRW, while electrode's voltage response in CS was < 50 mV throughout the experiment. These responses suggested that the high salt in CS suppressed the release of Ag^+ ions to solution, possibly due to the near-complete transformation to larger-sized but relatively monodisperse suspension compared to the MHRW. In particular, the similar response of the ISE in MHRW and DI may reflect the existence of minor populations of smaller particles (approximately 30-40 nm) to release Ag ions.

Figure 3. Potentiometric response of the silver ion-specific electrodes to the nAg suspension in different media

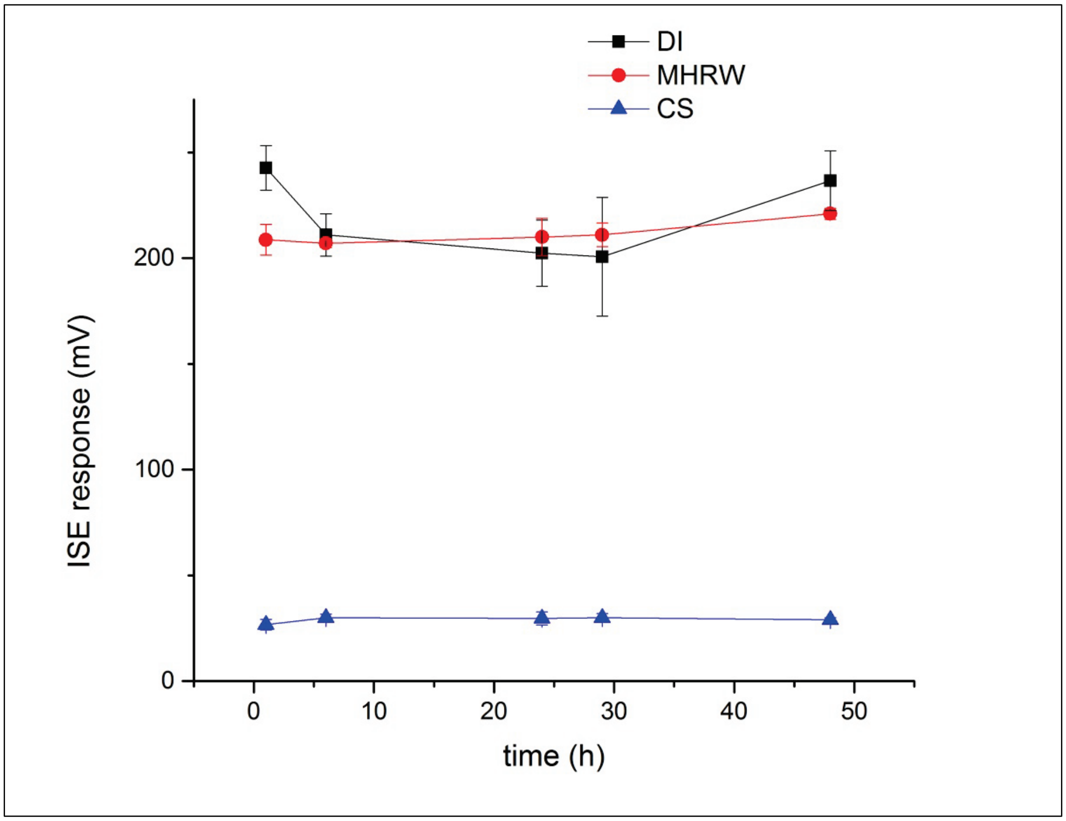

In addition to measuring Ag ions, the total concentration of Ag in solution both before and after ultracentrifuging suspension subsamples was also measured. Measurements made after ultracentrifugation represent the total dissolved Ag released into solution from the nAg suspension. The data (Figure 4) shows that the nAg suspension exhibited a low potential for dissolution, with dissolved Ag concentrations remaining fairly constant (thus, avoiding application of a kinetic dissolution model) and did not exceed 20 $\mu g\ L^{-1}$ over the 50-h time period. The difference in Ag concentration before and after ultracentrifugation represented the total Ag particles in solution. Based on equation 10, Ns of particles were estimated as 10^{12}, 10^{9}, and 10^{8} m^{-3} for the DI, MHRW, and CS media, respectively.

Figure 4. Measured Ag in solution with time from the nAg particles suspended in different media types. Data is shown for Ag concentration measured before and after ultracentrifugation of collected subsamples with time.

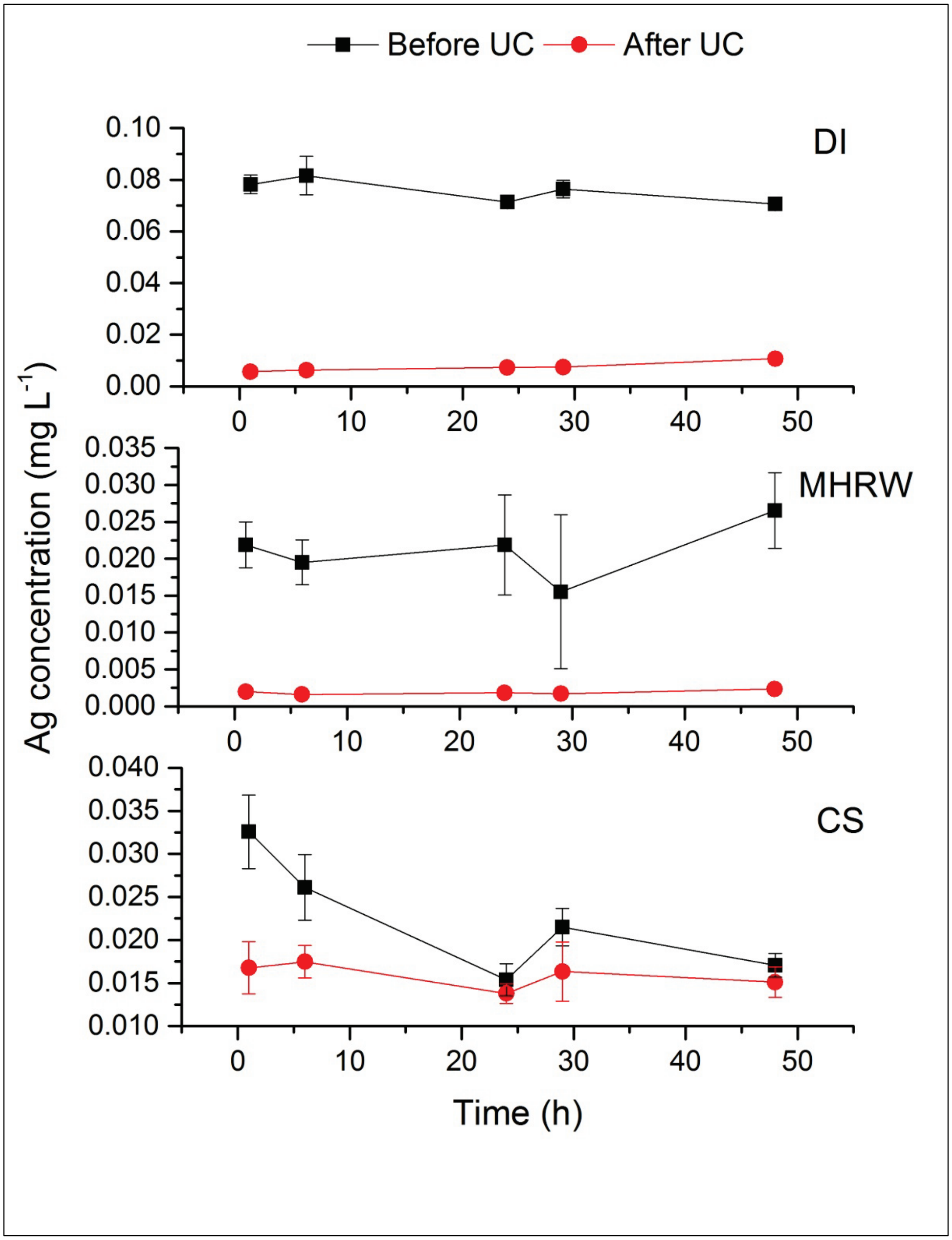

7.3 QA/QC Considerations

The techniques applied in this report are more reliable for “well-behaved” suspensions – a difficult achievement in environmental systems. Thus, the utility of these techniques in assessing the dispersion or dissolution potential of suspended nanomaterials relies on their careful, diagnostic application. While microscopy represents the only available method for measuring particle size, this is very labor intensive and prone to artifacts. Other methods for determining particle size are indirect with dimensions made by way of indirect processes. Thus, these methods must be utilized judiciously and with as much information regarding the tested matrix. We demonstrated the ability of DLS to provide particle size information regarding a dispersion in environmentally relevant media only if the correlogram is carefully inspected and the autocorrelation function is described with the appropriate model. The challenges of transmission-based turbidity measurements were demonstrated. Direct measurements of dissolved Ag proved challenging using electropotential methods (i.e., ISE). On the other hand, ultracentrifugation appeared to be very useful in distinguishing between particulate and dissolved Ag forms but requires expensive and specialized equipment.

References

Chappell, M. A., L. S. Miller, A. J. George, C. L. Price, J.-D. Mao, A. J. Bednar, J. M. Seiter, A. J. Kennedy, and J. A. Steevens. 2011. Simultaneous dispersion-dissolution of concentrated silver nanoparticle suspensions in the presence of model organic compounds. *Chemosphere* 84: 1108-1116.

Goodwin, J. W. 2009. Colloids and Interfaces with Surfactant and Polymers. 2nd ed. Chichester, Western Sussex, U.K.: John Wiley & Sons, Inc.

Kennedy, A. J., S. Diamond, J. K. Stanley, J. Coleman, J. A. Steevens, M. A. Chappell, J. G. Laird, and A. Bednar. 2014. Nanomaterials Ecotoxicology: a case study with nanosilver. In *Nanotechnology Environmental Health and Safety: Risks, Regulation and Management Accepted for Publication*, ed. Hull, M. S. and D. Bowman.

Kimijima, K., and T. Sugimoto. 2004. Growth mechanism of AgCl nanoparticles in a reverse micelle system. *Journal of Physical Chemistry B* 108: 3735-3738.

Langberg, D. E., and M. Nilmani. 1996. The production of nickel-zinc alloys by powder injection. *Metallurgical and Materials Transactions B* 27(5): 780-787.

Morrison, I. D., and S. Ross. 2002. Colloidal dispersions: suspensions, emulsions, and foams. New York: John Wiley & Sons, Inc.

Ottewill, R. H. 1990. Colloidal properties of latex particles. In *Scientific Methods for the Study of Polymer Colloids and their Applications*, ed. Candau, F., and R. H. Ottewill. The Netherlands: Kluwer Academic Publishers.

Sorensen, C. M. 1997. Scattering and absorption of light by particles and aggregates. In *Handbook of Surface and Colloid Chemistry*, ed. K. S. Birdi. Boca Raton, FL: CRC Press, LLC.

U.S. Environmental Protection Agency (USEPA). 2009. Test methods for evaluating solid waste, physical and chemical methods (SW-846): Method 6020 for ICP-MS.

Appendix A: Notes and Supplementary Data

Figure A1. Corellograms calculated from the integrated light scattering response of the nAg suspensions. Error bars show the analytical uncertainty among 6 replicate samples.

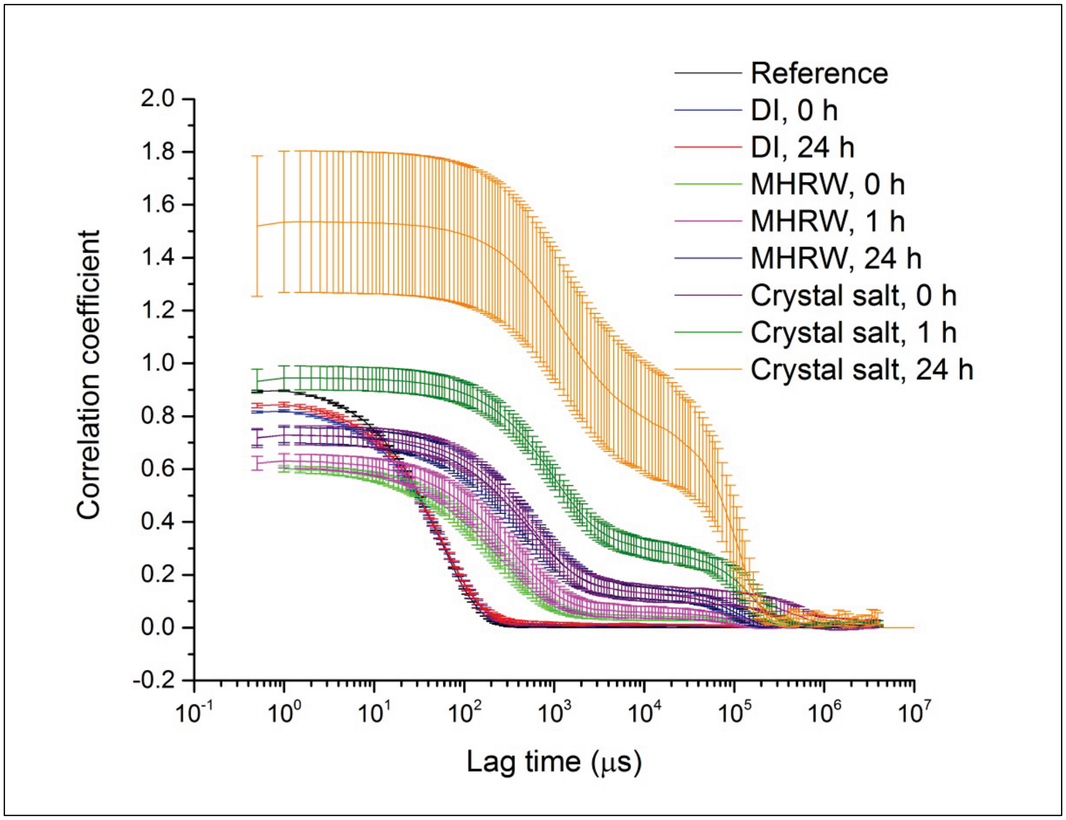

Figure A2. Calibration curve generated for the Ag ion-specific electrode.

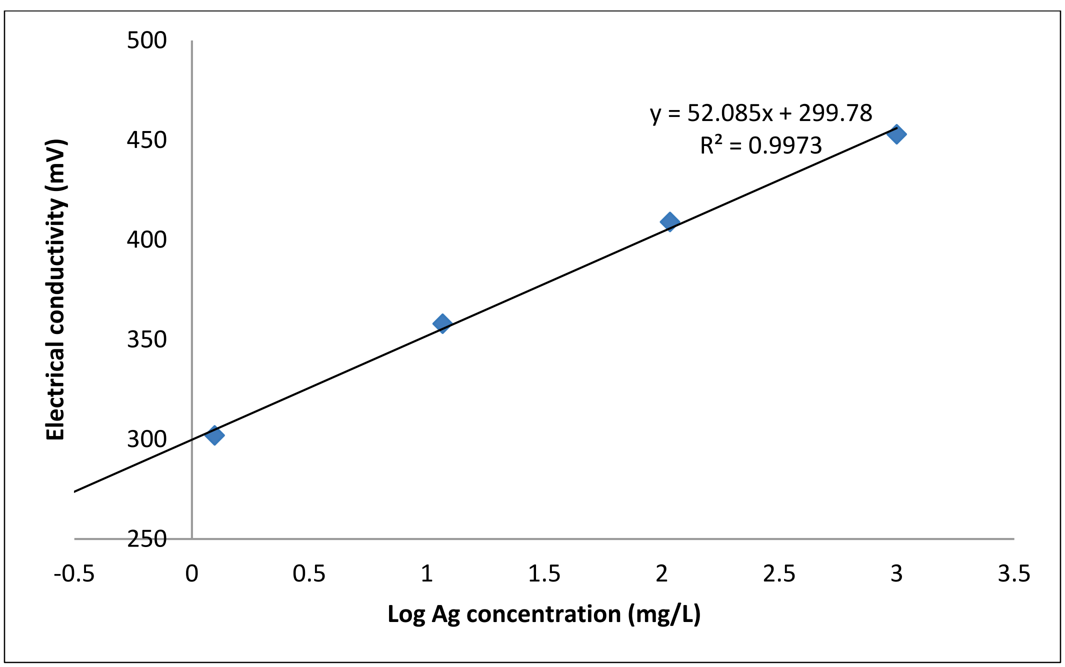

REPORT DOCUMENTATION PAGE

Form Approved OMB No. 0704-0188

1. REPORT DATE *(DD-MM-YYYY)*
May 2016

2. REPORT TYPE
Final report

3. DATES COVERED *(From - To)*

4. TITLE AND SUBTITLE
Nanomaterial Dispersion/Dissolution Characterization: Scientific Operating Procedure SOP-F-1

5a. CONTRACT NUMBER

5b. GRANT NUMBER

5c. PROGRAM ELEMENT NUMBER

6. AUTHOR(S)
Lesley F. Miller, Mark A. Chappell

5d. PROJECT NUMBER

5e. TASK NUMBER

5f. WORK UNIT NUMBER

7. PERFORMING ORGANIZATION NAME(S) AND ADDRESS(ES)
U.S. Army Engineer Research and Development Center, Environmental Laboratory
3909 Halls Ferry Road, Vicksburg, MS 39180-6199

8. PERFORMING ORGANIZATION REPORT NUMBER
ERDC/EL SR-16-1

9. SPONSORING / MONITORING AGENCY NAME(S) AND ADDRESS(ES)
Headquarters, U.S. Army Corps of Engineers
Washington, DC 20314-1000

10. SPONSOR/MONITOR'S ACRONYM(S)

11. SPONSOR/MONITOR'S REPORT NUMBER(S)

12. DISTRIBUTION / AVAILABILITY STATEMENT
Approved for public release; distribution unlimited.

13. SUPPLEMENTARY NOTES

14. ABSTRACT

Evidence suggests that a material's dispersion and dissolution behaviors may be crucial to understanding the material's environmental risk. Since exposure risks are directly determined by the environmental fate of nano silver (nAg), extensive efforts have been put forth in elucidating the behavior of these materials in natural systems. Thus, it is important to understand the different metrics that can be used to represent nanoparticles (NPs) in a system. Given the connection between a material's dispersion and dissolution kinetics, a protocol is presented to measure the dissolution kinetics of nanomaterials using a simple 48-hour experimental protocol that utilizes environmentally representative waters as well as non-destructive analytical techniques. Protocols for the simultaneous measurement of the nanoparticle dispersion properties are also presented. When used with the appropriate equations listed in this scientific operating procedure, data derived from these simple experiments can provide fundamental information about the behavior of nanoparticles in different environments.

15. SUBJECT TERMS
Nanoparticles
Dispersion
Dissolution
Fate
Kinetics

16. SECURITY CLASSIFICATION OF:			17. LIMITATION OF ABSTRACT	18. NUMBER OF PAGES	19a. NAME OF RESPONSIBLE PERSON
a. REPORT	b. ABSTRACT	c. THIS PAGE			19b. TELEPHONE NUMBER *(include area code)*
UNCLASSIFIED	UNCLASSIFIED	UNCLASSIFIED		35	